

**A global investigation of phase equilibria using the
Perturbed-Chain Statistical-Associating-Fluid-Theory
(PC-SAFT) approach**

Leonid Yelash^a, Marcus Müller^b, Wolfgang Paul^a, Kurt Binder^a

^a *Institute of Physics, WA 331, Johannes-Gutenberg University, D-55099 Mainz, Germany*

^b *Department of Physics, University of Wisconsin,*

1150 University Avenue, Madison, WI 53706

(Dated: October 22, 2018)

Abstract

The recently developed Perturbed-Chain Statistical Associating Fluid Theory (PC-SAFT) is investigated for a wide range of model parameters including the parameter m representing the chain length and the thermodynamic temperature T and pressure p . This approach is based upon the first-order thermodynamic perturbation theory for chain molecules developed by Wertheim [M. S. Wertheim, J. Stat. Phys. **35**, 19–46 (1984); *ibid.* **42**, 459–492 (1986)] and Chapman *et al.* [G. Jackson, W. G. Chapman and K. E. Gubbins, Mol. Phys. **65**, 1 (1988); W. G. Chapman, G. Jackson and K. E. Gubbins, *ibid.* **65**, 1057 (1988)] and includes dispersion interactions via the second-order perturbation theory of Barker and Henderson [J. Chem. Phys. **47**, 4714 (1967)]. We systematically study a hierarchy of models which are based on the PC-SAFT approach using analytical model calculations and Monte Carlo simulations. For one-component systems we find that the analytical model in contrast to the simulation results exhibits two phase-separation regions in addition to the common gas–liquid coexistence region: One phase separation occurs at high density and low temperature. The second demixing takes place at low density and high temperature where usually the ideal gas phase is expected in the phase diagram. These phenomena, which are referred to as “liquid–liquid” and “gas–gas” equilibria, give rise to multiple critical points in one-component systems, as well as to critical end points (CEP) and equilibria of three fluid phases, which can usually be found in multicomponent mixtures only. Furthermore, it is shown that the “liquid–liquid” demixing in this model is not a consequence of a “softened” repulsive interaction as assumed in the theoretical derivation of the model. Experimental data for the melt density of polybutadiene with molecular mass $M_w = 45000$ g/mol are correlated here using the PC-SAFT equation. It is shown that the discrepancies in modeling the polymer density at ambient temperature and high pressure can be traced back to the “liquid–liquid” phase separation predicted by the equation of state at low temperatures. This investigation provides a basis for understanding possible inaccuracies or even unexpected phase behavior which can occur in engineering applications of the PC-SAFT model aiming at predicting properties of macromolecular substances.

PACS numbers: 05.70.Ce, 05.70.Fh, 51.30.+i, 61.25.Hq, 64.10.+h, 64.60.Kw, 64.60.My, 64.70.Fx, 64.70.Ja, 83.80.Sg, 87.53.Wz

I. INTRODUCTION

The theoretical development of analytical models to predict the equation of state for polymer melts and solutions is a longstanding problem of polymer science and very important for engineering applications. As a consequence, much theoretical effort has already been directed towards this problem. The Flory–Huggins theory¹, for example, is based upon a regular solution model which in a very simple manner considers intermolecular interactions and chemical structure of molecules. This theory can analytically describe generic, universal features of polymer melts and solutions, e.g. the chain length dependence of the critical properties and phase equilibria with an upper critical solution temperature (UCST). Within this theory, however, the third and all higher order virial coefficients exclusively stem from the combinatorial entropy such that the monomer interactions and liquid structure (packing) is only incompletely described. Thus, the Flory-Huggins theory fails to describe, for instance, a lower critical solution temperature (LCST) and does not incorporate the compressibility (i.e., the pressure dependence of the density) of mixtures. Another approach is based upon equation-of-state description such as the Sanchez-Lacombe equation^{2,3} which can parameterize the compressibility of mixtures containing polymers.

In modern condensed matter science, however, one is dealing with more complicated theories which are able to provide a very accurate quantitative description of macromolecular systems. Particular successful is an approach pioneered by Wertheim^{4,5,6,7,8,9} and Chapman *et al.*^{10,11} based on liquid state theory. In the classical form of perturbation theory of (simple) fluids, one starts from the description of a reference fluid with purely repulsive interactions for which the equation of state and the pair correlation function, $g(r)$, are rather accurately known. Using the thermodynamic and structural properties of the repulsive reference fluid as input, one treats the attractive interactions as a perturbation^{12,13,14,15}. In contrast to this approach for simple fluids, the thermodynamic perturbation theory for chain molecules (TPT1)^{4,5,6,7,8,9,10,11} employs the corresponding fluid of un-connected monomers as starting point (a reference fluid), and treats the chain connectivity as perturbation.

The first engineering application of this first order thermodynamic perturbation theory has become well-known under the name “Statistical Associating Fluid Theory” (SAFT)^{16,17} and this name denotes any implementation of the TPT1 method. This approach has been extensively developed further^{18,19} into several distinct variants. For example, using a square-

well potential of variable range (VR), the SAFT-VR method has been proposed^{20,21} while the SAFT-LJ²² and the soft-SAFT^{23,24} methods use a Lennard-Jones fluid as reference system. The TPT1-MSA method^{25,26} also utilizes the Lennard-Jones fluid as a reference system which can be analytically described within the mean spherical approximation. Finally, the Perturbed-Chain SAFT (PC-SAFT) method^{27,28,29,30} has been recently proposed which is based upon a hard chain reference system augmented by an attractive interaction derived from the Barker and Henderson perturbation approach^{12,13,14,15} extended to chain molecules with additional adjustment to experimental data. This model has attracted great attention due to its industrial relevance as a modeling and predicting tool, for example, for polar fluids (e.g. hydrofluoroethers)³¹, polymer fractionation³², as well as a theoretically sound equation of state for investigating barotropic phase phenomena in binary fluid systems³³ and predicting the phase behavior in ternary and quaternary systems³⁴. Furthermore, a simplified version of the PC-SAFT model has been proposed recently³⁵ which is based on the Carnahan-Starling equation for hard spheres³⁶. Therefore, it is not only of theoretical interest but also of practical relevance to carry out a global investigation of the phase behavior which can be predicted by the PC-SAFT approach, and to test its accuracy by comparison with Monte Carlo simulations for precisely the same model.

II. EQUATION-OF-STATE MODEL

A detailed description and derivation of the original PC-SAFT model can be found elsewhere^{27,28,29}. Here we briefly give an introduction into the PC-SAFT approach for chain molecules.

In the perturbation approach¹², the Helmholtz free energy of a system of molecules can be expressed as a sum of the contributions from an unperturbed (reference) system where particles only interact via repulsive forces and a perturbation due to attractive interactions (dispersion forces):

$$\frac{A}{Nk_{\text{B}}T} = \frac{A^{\text{ref}}}{Nk_{\text{B}}T} + \frac{A^{\text{disp}}}{Nk_{\text{B}}T} \quad (1)$$

where “ref” and “disp” denote the contributions of the unperturbed reference system and the dispersion perturbation, respectively.

A. Reference Hard-Chain Fluid

In PC-SAFT, the reference, unperturbed system is the same as in SAFT: It is a chain fluid composed of hard spheres. The Helmholtz free energy of the hard-chain system is given within the TPT1 formalism by:

$$\frac{A^{\text{ref}}}{Nk_{\text{B}}T} = \frac{A^{\text{id}}}{Nk_{\text{B}}T} + \bar{m} \frac{A^{\text{hs}}}{Nk_{\text{B}}T} + \sum_i x_i (m_i - 1) \frac{A_i^{\text{chain}}}{Nk_{\text{B}}T} \quad (2)$$

where $\bar{m} = \sum_i x_i m_i$ is an average number of segments in a multi-component mixture of chain molecules; m_i are the segment numbers for the chains of component i . For one-component chain fluids with segment number m this expression simplifies to:

$$\frac{A^{\text{ref}}}{Nk_{\text{B}}T} = \frac{A^{\text{id}}}{Nk_{\text{B}}T} + m \frac{A^{\text{hs}}}{Nk_{\text{B}}T} + (m - 1) \frac{A^{\text{chain}}}{Nk_{\text{B}}T} \quad (3)$$

Here A^{id} is the Helmholtz free energy of the ideal gas system; A^{hs} is the residual hard-sphere contribution due to the reduction of the system free volume by the volume of monomers; A^{chain} is the contribution to the Helmholtz free energy due to formation of bonds between the monomers, which can be calculated from the contact value of the pair correlation function of the reference hard sphere fluid. For a multi-component mixtures one obtains:

$$\frac{A^{\text{chain}}}{Nk_{\text{B}}T} = -\ln g_{ij}^{\text{hs}} \quad (4)$$

The free energy, the compressibility factor, and the contact pair correlation functions g_{ij}^{hs} for components i and j of the hard-sphere mixture are modeled in PC-SAFT using the BMCSL equation of state derived by Boublík³⁷ and Mansoori et al.³⁸:

$$\frac{A^{\text{hs}}}{Nk_{\text{B}}T} = \frac{1}{\zeta_0} \left[\frac{3\zeta_1\zeta_2}{1-\zeta_3} + \frac{\zeta_2^3}{\zeta_3(1-\zeta_3)^2} + \left(\frac{\zeta_2^3}{\zeta_3^2} - \zeta_0 \right) \ln(1-\zeta_3) \right] \quad (5)$$

$$Z^{\text{hs}} = \frac{1}{1-\zeta_3} + \frac{3\zeta_1\zeta_2}{\zeta_0(1-\zeta_3)^2} + \frac{3\zeta_2^3 - \zeta_3\zeta_2^3}{\zeta_0(1-\zeta_3)^3} \quad (6)$$

$$g_{ij}^{\text{hs}} = \frac{1}{1-\zeta_3} + \left(\frac{d_i d_j}{d_i + d_j} \right) \frac{3\zeta_2}{(1-\zeta_3)^2} + \left(\frac{d_i d_j}{d_i + d_j} \right)^2 \frac{2\zeta_2^2}{(1-\zeta_3)^3} \quad (7)$$

where

$$\zeta_n = \frac{\pi}{6} \rho \sum_i x_i m_i d_i^n \quad \text{for } n = 0, 1, 2, 3 \quad (8)$$

These equations have been derived in a similar way as the Carnahan–Starling equation³⁶, however starting from the solutions of the Percus–Yevick integral equation for mixtures of hard spheres. For a one-component system, these equations simplify to the Carnahan–Starling hard-sphere equations:

$$\frac{A^{\text{CS}}}{Nk_{\text{B}}T} = \frac{4\eta - 3\eta^2}{(1 - \eta)^2} \quad (9)$$

$$Z^{\text{CS}} = \frac{1 + \eta + \eta^2 - \eta^3}{(1 - \eta)^3} \quad (10)$$

$$g_{\sigma}^{\text{CS}} = \frac{2 - \eta}{2(1 - \eta)^3} \quad (11)$$

with the packing fraction

$$\eta = \frac{\pi}{6} \rho m d^3 \quad (12)$$

B. Attractive Interactions

The segments of the chain molecules can exert attractive forces onto each other. This attraction acts between segments of the same molecule as well as between different chains. Within the perturbation approach, the Helmholtz free energy of a system with attractive interactions can be expanded in a power series of the inverse temperature, $\beta = 1/(k_{\text{B}}T)$, which is the high-temperature expansion. The exact Helmholtz free energy is therefore described by the infinite sum of terms which represent the contributions of different orders. In the infinite-temperature limit, $\beta \rightarrow 0$, all the terms in this expansion vanish except the zero-order term which corresponds to a reference fluid without attractive interactions, i.e., an unperturbed system. If this expansion is truncated after the term of order β^2 , it is called the second order perturbation theory, which for simple fluids of spherical molecules with a hard-sphere reference fluid has been derived by Barker and Henderson^{13,14}. In the

second-order approximation, the Helmholtz free energy of a dispersion interaction is given by:

$$\frac{A^{\text{disp}}}{Nk_{\text{B}}T} = \frac{A_1}{Nk_{\text{B}}T} + \frac{A_2}{Nk_{\text{B}}T} \quad (13)$$

The first-order term, A_1 , in the perturbation expansion can be related to an average of the number of segment pairs within the range of the attractive interaction. The higher-order terms are related to higher moments of the distribution of this number. Alder *et al.*³⁹ have investigated a fourth order perturbation theory and shown that this quantity is nearly Gaussian distributed. If the distribution were exactly normal, the second order perturbation theory would be exact. In the close-packing and the low-density limits, the deviations from the normal distribution vanish. Thus, one expects the second order perturbation theory to be accurate at high density and low temperature, provided that the above mentioned distribution is nearly normal and the perturbation terms well determined.

The perturbation contributions in PC-SAFT are expressed by equations which depend on the chain length parameter m (differing from the perturbation theory of spherical molecules):

$$\frac{A_1}{Nk_{\text{B}}T} = -2\pi\rho\frac{\epsilon}{k_{\text{B}}T}m^2\sigma^3 I_1(\rho, m) \quad (14)$$

$$\frac{A_2}{Nk_{\text{B}}T} = -\pi\rho m \left[\frac{\partial}{\partial \rho} \rho(1 + Z^{\text{hc}}) \right]^{-1} \left(\frac{\epsilon}{Nk_{\text{B}}T} \right)^2 m^2\sigma^3 I_2(\rho, m) \quad (15)$$

where Z^{hc} is the residual compressibility factor of the reference hard-chain fluid, which can be calculated from Eqs. (3)-(7). The perturbation integrals, $I_1(\rho, m)$ and $I_2(\rho, m)$, implicitly depend on density and chain length parameter, ρ and m . Actually, these integrals can be calculated from the pair correlation function, which in turn depends on density and chain length:

$$I_1(\rho, m) = \int_1^\infty \tilde{u}_1(x) g^{\text{hc}}(x') x^2 dx \quad (16)$$

$$I_2(\rho, m) = \int_1^\infty \tilde{u}_1(x)^2 g^{\text{hc}}(x') x^2 dx \quad (17)$$

where $\tilde{u}_1 = u_1/\epsilon$ is a normalized attraction potential; u_1 is the attractive (perturbation) part of a potential; $x = r/\sigma$ describes the distance between segments normalized by the

temperature-independent segment diameter σ . The distance normalized by the temperature-dependent segment diameter is denoted by $x' = r/d(T)$. $g^{\text{hc}}(x)$ is the segment-segment pair correlation function of hard-chain molecules.

The analytical evaluation of the integrals, $I_1(\rho, m)$ and $I_2(\rho, m)$, which are required for the perturbation theory, is difficult. Firstly, it requires analytical expressions for the pair correlation functions of the hard-chain fluid that are reliable over the entire range of density and chain length parameter. These expressions can be obtained from integral-equation theories for monomers and short chains^{40,41,42,43,44}. However, because of non-trivial correlations due to excluded volume effects, such expressions become less accurate for long chains and polymers, where for instance m can be of order 10^3 and larger. Secondly, the integrals additionally depend on the interaction potential, \tilde{u}_1 . For the special case of square-well interactions, which do not depend on the intermolecular distance r in the range of the attraction well $\sigma < r < \lambda\sigma$, the integrals simplify: They depend on the pair correlation function only and there is a simple relation between the integrals:

$$I_2(\rho, m) = \frac{\partial}{\partial \rho} [\rho I_1(\rho, m)] \quad (18)$$

For a general form of the intermolecular potential, however, the perturbation integrals are non-trivial functions. A numerical calculation of such integrals is often omitted in engineering applications for practical reasons. In PC-SAFT one follows an approach previously proposed for monomers and dimers^{45,46} and approximates these integrals by a power series of sixth order in the packing fraction:

$$I_1(\eta, m) = \sum_{i=0}^6 a_i(m) \eta^i \quad (19)$$

$$I_2(\eta, m) = \sum_{i=0}^6 b_i(m) \eta^i \quad (20)$$

where η is the packing fraction, defined in Eq. (12). For chain molecules, the coefficients $a_i(m)$ and $b_i(m)$ depend on the number of segments m . This chain length dependence is approximated by following expressions in PC-SAFT:

$$a_i(m) = a_{0i} + \frac{m-1}{m} a_{1i} + \frac{m-1}{m} \frac{m-2}{m} a_{2i} \quad (21)$$

$$b_i(m) = b_{0i} + \frac{m-1}{m}b_{1i} + \frac{m-1}{m}\frac{m-2}{m}b_{2i} \quad (22)$$

Eqs. (1), (3)–(15), and (19)–(22) define the PC-SAFT approach to chain molecules. For equations Eqs. (19)–(22) one needs no less than 42 model constants, a_{ij} and b_{ij} . These are universal constants, in the sense that these parameters do not depend on a specific substance to be modeled, but represent the properties of a certain class of intermolecular potential function, e.g. the square-well potential, the Lennard-Jones potential or real interactions.

Generally, Eqs. (19)–(22) represent a two-dimensional frame with a set of constants, a_{ij} and b_{ij} , which can be fitted to any perturbation. In the course of the derivation of the PC-SAFT approach, two sets of constants, a_{ij} and b_{ij} , have been obtained by the fitting the model to the square-well potential^{27,47} (which is called SW-PC-SAFT here) or to real substances for PC-SAFT^{27,28}. This is particularly useful because on the one hand, substituting the parameter set, a_{ij} and b_{ij} , one can use the PC-SAFT approach to describe the behavior of a specific perturbation potential (e.g. the square-well potential) and one can test the accuracy of this perturbation approach by quantitative comparison with computer simulations of exactly the same model. On the other hand, using the parameter set, a_{ij} and b_{ij} , obtained for real substances, one can compare the model to Monte Carlo simulations of a coarse-grained potential for chain molecules, e.g. the “bead-spring” model which has been successfully applied to model real systems^{48,49}.

C. “Softened” Repulsion

The hard-sphere repulsion is a very simple approximation and it only provides a very crude description of repulsive interaction in real systems. A more realistic representation of real interactions is, for example, the Lennard-Jones potential. For modeling the Lennard-Jones repulsion, Barker and Henderson¹⁴ proposed an effective, temperature-dependent diameter $d(T)$ which is based on the hard-sphere reference fluid diameter σ :

$$d(T) = \int_0^\sigma [1 - \exp(-\beta u(r))] dr \quad (23)$$

Using a pair potential $u(r)$ one can calculate from Eq. (23) the temperature-dependent diameter not only for a truly soft potential, e.g. the Lennard-Jones potential, but also for “softened” potentials like the Chen-Kreglewski potential⁵⁰. The Chen-Kreglewski potential

has an additional repulsive step if compared to the square-well potential. It is shown in Fig. 1. Using the Barker-Henderson recipe for the Chen-Kreglewski potential, one obtains a temperature-dependent effective diameter⁵⁰:

$$d(T) = \sigma [1 - 0.12 \exp(-3\epsilon\beta)] \quad (24)$$

At low temperature, the effective diameter approaches the hard-sphere diameter $d(T \rightarrow 0) \rightarrow \sigma$. In the high-temperature limit, the effective diameter is smaller than the hard-sphere diameter $d(T \rightarrow \infty) \rightarrow 0.88\sigma$. The temperature-dependence of the effective diameter for the Chen-Kreglewski potential is shown in Fig. 2.

In the PC-SAFT approach, the hard-sphere repulsion is replaced by the “softened” repulsion of the Chen-Kreglewski potential, which is modeled by substituting expression Eq. (24) for the diameter d . This method has also been employed earlier for the BACK⁵⁰ equation and the SAFT⁵¹ equation. In SW-PC-SAFT⁴⁷, in contrast, the repulsion is treated as for the hard-sphere fluid: The segment diameter, $d = \sigma$, does not change with temperature.

III. DIFFERENT LEVELS IN THE PC-SAFT APPROACH

It has been mentioned above that in the PC-SAFT approach to chain molecules there are two approximations which describe the shape of the interaction potential: i) The effective temperature-dependent diameter of segments, $d(T)$, models the repulsive branch of the potential curve; ii) The polynomial expansion with a set of universal constants, a_{ij} and b_{ij} , approximates the attractive part of the potential. These approximations introduce into the model flexibility for adapting it to different intermolecular potentials. Therefore, we can build here a hierarchy of models which can be derived from the PC-SAFT perturbation approach. The levels in this hierarchy correspond to complexity of the interaction potential, if compared to the reference-model potential. The level 0 represents the reference hard-chain fluid.

Level 1) SW-PC-SAFT: The Square-Well Perturbed-Chain SAFT is based on the square-well potential. The universal constants, a_{ij} and b_{ij} , for the perturbation polynomials, $I_1(\rho, m)$ and $I_2(\rho, m)$, have been obtained by fitting the model to the square-well potential⁴⁷. The hard-sphere diameter, d , is constant in this model.

Level 2) CK-PC-SAFT: The Chen-Kreglewski Perturbed-Chain SAFT is similar to

SW-PC-SAFT except that the Chen-Kreglewski repulsion is modeled instead of the hard-sphere repulsion. As a consequence, the effective, temperature-dependent diameter given by Eq. (24) is substituted for the diameter d . In order to model the square-well attraction of the Chen-Kreglewski potential, the same set of the universal constants, a_{ij} and b_{ij} , is employed for the perturbation polynomials as in SW-PC-SAFT.

Level 3) PC-SAFT: This model includes the effective temperature-dependent diameter for the Chen-Kreglewski repulsion (Eq.24) and the universal constants, a_{ij} and b_{ij} , obtained by fitting the model to real substances²⁸.

One particular advantage of this hierarchical approach is that not only the final result – the equation of state – but also the different approximations at various stages of the analytical treatment can be evaluated. In the first two equation-of-state models (levels 1 and 2), the interaction potential is well defined: It is the square-well chain for the SW-PC-SAFT model and the Chen-Kreglewski chain for the CK-PC-SAFT model. For these models one can carry out Monte Carlo simulations of chain molecules for exactly the same interaction potentials and thus assess the quantitative accuracy of the perturbed-chain approach. In the third model (PC-SAFT), only the “softened” repulsion is well defined, whereas the dispersion interaction has resulted from a fitting procedure to real substances. Thus, we additionally perform Monte Carlo simulations of a coarse-grained “bead-spring” model for chain molecules, which is able to reproduce many properties of real substances^{48,49}. These simulation models and techniques are described in the following part.

A. Bead-Spring Model for Chain Molecules

The bead-spring model for chain molecules is based upon the shifted Lennard-Jones (LJ) and the Finitely Extensible Nonlinear Elastic (FENE) potential^{48,52,53}. This model is schematically depicted in Fig.3. The Lennard-Jones potential describes the repulsion and dispersion forces between the segments for both the intermolecular and non-bonded intramolecular interactions:

$$U_{LJ}(r) = 4\epsilon \left[\left(\frac{\sigma}{r} \right)^{12} - \left(\frac{\sigma}{r} \right)^6 \right] + \frac{127}{4096}\epsilon \quad (25)$$

The Lennard-Jones potential has formally an infinite range. In order to increase the efficiency of computer simulations, one can reduce the interaction range of the potential.

This does not change the qualitative phase behavior and there are different ways how to do that.⁵⁴ Here we use the cut-off distance at $r_{\text{cutoff}} = 2\sqrt[6]{2}\sigma$ ^{48,53}, which is close to the minimum of the pair correlation function beyond the second correlation shell in the dense phase, thus minimizing the error of cutoff. Furthermore, the potential is shifted in order to avoid the energy discontinuity at the cut-off distance.

Additionally, the segments bonded along a chain molecule interact via the FENE potential. In our coarse-grained bead-spring model, the distance between the bonded segments can change to a certain extent, e.g. upon variation of the pressure. There is an equilibrium distribution of bond lengths for fixed thermodynamic parameters. The stretching of the bonds is restricted by introducing a bond-energy penalty, which diverges for the bond length equal to $r = 1.5\sigma$:

$$U_{\text{FENE}}(r) = -33.75\epsilon \ln \left[1 - \left(\frac{r}{1.5\sigma} \right)^2 \right] \quad (26)$$

This choice of the constants in the FENE potential favors the maxima of the distance distribution for the bonded and non-bonded monomers at $r \approx 0.96\sigma$ and $r \approx 1.12\sigma$, respectively. The repulsion between the bonded segments is modeled by the Lennard-Jones potential. In combination, the Lennard-Jones and the FENE potentials

$$U_{\text{LJ+FENE}}(r) = U_{\text{LJ}}(r) + U_{\text{FENE}}(r) \quad (27)$$

exhibit a sharp minimum of the potential energy at an equilibrium value of the bond length (see Fig.3).

This bead-spring model is very well studied and has already been applied to many different problems including, recently, the coarse-grained modeling of polymer solutions^{48,49}. It has been shown, for example, that this model predicts phase behavior for mixtures of carbon dioxide/hexadecane which is in good agreement with experimental data.

B. Chen-Kreglewski Chain Molecules

The “softened” repulsion of the Chen-Kreglewski potential is the theoretical basis for the PC-SAFT equation. Therefore, it is investigated here using computer simulations. The potential is shown schematically in Fig. 1. It is similar to the square-well potential, however

it has an additional repulsive step (inverse well):

$$U_{\text{CK}}(r) = \begin{cases} +\infty & : r < \sigma - 0.12 \\ +3\epsilon & : \sigma - 0.12 < r < \sigma \\ -\epsilon & : \sigma < r < \lambda\sigma \\ 0 & : \lambda\sigma < r \end{cases} \quad (28)$$

The height $+3\epsilon$ and the width 0.12σ of the repulsion step were empirically determined in order to improve the description of the equation of state for some small molecules, e.g. noble gases and short alkanes⁵⁰. From a comparison shown in Fig. 4 one can see that the Chen-Kreglewski potential is a rather crude approximation of realistic interactions, e.g. the Lennard-Jones potential. The interaction range of the Chen-Kreglewski potential is 1.5σ , which is by factor ≈ 1.5 smaller than the cutoff distance of the Lennard-Jones potential, if the range and energy parameters, σ and ϵ , are taken the same in $U_{\text{LJ}}(r)$ and $U_{\text{CK}}(r)$.

In order to perform the Monte Carlo simulations of the Chen-Kreglewski potential and to compare directly with the PC-SAFT approach, the computer code, which has been developed in the Condensed Matter Theory Group at the University of Mainz for the Lennard-Jones+FENE model⁵⁵, was generalized to different interaction potentials. For modeling chain molecules with the Chen-Kreglewski potential, the monomers are connected by rigid bonds. Monte Carlo simulations of precisely the same interaction potential can therefore be carried out and quantitatively compared to the analytical calculations with the CK-PC-SAFT model in order to establish the accuracy of the perturbed-chain approach. The CK-PC-SAFT equation represents level 2 in the hierarchy of the PC-SAFT approach described above.

C. Square-Well Chain Molecules

The square-well chain-molecule model represents the level 1 in the hierarchy of the models derived from the PC-SAFT approach: It is a theoretical basis for the SW-PC-SAFT equation⁴⁷. For a systematic investigation of this approach, Monte Carlo simulations of square-well chain molecules and monomers are also included in our investigation. In this model, the segments of chain molecules are connected by the rigid bonds of length σ and interact via a square-well potential of the range $\lambda = 1.5\sigma$. Thus, the simulations are carried

out for precisely the same interaction potential as in the SW-PC-SAFT equation of state.

IV. COMPUTATIONAL DETAILS

A. Simulation Techniques

Monte Carlo simulations are performed here with the *NPT* simulation technique to obtain equation of state for chain molecules and for monomers rather than to use the *NVT* method or to calculate phase coexistence from the Gibbs ensemble simulations. The *NPT* method can be used to investigate both the equation of state as well as the first order transitions⁵⁶, whereas in the *NVT* simulations the system can stay in a metastable state, e.g. at negative pressure. However, *NPT* simulations take longer than *NVT* simulations due to volume fluctuations.

The equation of state from the simulations can readily be compared to the predictions of the PC-SAFT model. We did not systematically study finite size effects in the simulations. Experience with related models^{48,49} has shown that finite size effects are negligible except in the intermediate vicinity of critical points. In the present paper, only data in the one-phase region away from critical points are presented. Thus we do not expect finite size effects to affect our conclusions.

The chain length $m = 29$ beads per chain has been chosen because such chains can be equilibrated in relatively short simulation runs, and they are still long enough to represent the key features of polymer molecules. It has also been chosen for a compatibility reason to other extensive studies of a polybutadiene melt using atomistic molecular dynamic simulations^{57,58}. In the bead-spring model investigation, the simulation box contains 160 chain molecules. For the square-well and Chen-Kreglewski models, 40 molecules per box are used. The simulations of monomers ($m = 1$) are carried out using 1562 particles in the simulation box. The initial configurations are generated using the configurational bias Monte Carlo method⁵⁶. At low and moderate density one can generate an initial configuration by inserting the molecules into the simulation box until a desired density is reached. At high density, the probability to successfully insert a long chain molecule decreases rapidly. However, one can start inserting the molecules into a larger box and afterwards compress the box (e.g. in *NPT* runs) in order to increase the density. After generating an initial configuration, it is equilibrated

using periodic boundary conditions until the system properties (e.g. density and energy) fluctuate around a constant value. The equilibration time can vary largely depending on the state parameters (temperature and density). At low density, the equilibration time is usually very short and the system can be brought into an equilibrium state after several MC steps. At high density and low temperature, however, the relaxation processes slow down rapidly and the equilibration time can be several millions Monte Carlo steps. After reaching an equilibrium state, *NPT* simulations are performed in order to obtain good statistics of measured quantities. We have also done a series of *NVT* simulations for testing and compatibility reasons. However, the pressure fluctuations in *NVT* simulations can sometimes exceed the value of the pressure, whilst the *NPT* method provides high accuracy of the measured density and there is no need for the virial expression for the pressure.

In *NPT* simulations, the volume of the simulation box is changed by Monte Carlo moves at constant pressure and temperature. In addition to the volume change, the chain conformations are modified by displacements which include local monomer moves and reptation of the entire chain. In a local move, each monomer of a molecule is tried once. In a reptation move, the monomer at one molecule end, which is chosen randomly, is cut and attached to the opposite end of the same molecule. This procedure is repeated for all molecules in the simulation box. The number of moves in one Monte Carlo step can be varied. The typical choice for the simulations here is one volume change, one local move and 100 reptations in one Monte Carlo step. At high density ($\rho^* \geq 1$), the acceptance probability of the reptation moves can decrease strongly; hence, the number of the reptation moves in one Monte Carlo step is set to a lower value (10 or 1) in such cases. For the same reason, the insertion of an entire chain molecule is practically impossible at high densities.

B. Calculating Phase Diagrams

Using equation-of-state models, we calculate isotherms, spinodals, phase equilibria and critical points. The pressure, p , (e.g. for the isotherms) can be calculated in a straightforward way by substituting the temperature, T , and the density, ρ , (or the molar volume, v) into an equation of state. This calculation method is free of errors (except numerical rounding errors). Phase equilibria, spinodals and critical points are calculated by iteratively searching for state points that fulfill the corresponding thermodynamic conditions. After the

convergence of the iteration procedure, e.g. for the critical isotherms plotted in the figures, we explicitly verified by substituting the results in the equation of state or its derivatives that the solution fulfills the required conditions (i.e., that the convergence error is negligible).

The calculation of equilibrium of two phases at the same temperature, T , and pressure, p , is equivalent to solving the following set of two equations:

$$\left. \begin{aligned} \mu(\rho', T) - \mu(\rho'', T) &= 0 \\ p(\rho', T) - p(\rho'', T) &= 0 \end{aligned} \right\} \quad (29)$$

where ρ' and ρ'' are the densities of the coexisting phases being iterated to satisfy Eqs. (29). The pressure, p , is calculated from an equation of state. The expression for the chemical potential, μ , can be derived from an equation of state using thermodynamic relations. For a one-component system it is $\mu = f + pv$, with $f = -\int pdv$ being the Helmholtz free energy.

Two-phase equilibria in one-component systems have one degree of freedom ($d = 1$) according to the Gibbs Phase Rule:

$$d = c - ph + 2 \quad (30)$$

where $c = 1$ is the number of components and $ph = 2$ the number of phases at equilibrium. It follows that in Eqs. (29) one can freely vary only one of the variables: T , ρ' and ρ'' . For example, one can first fix the temperature, T , and obtain ρ' and ρ'' via iteration of Eqs. (29).

Spinodals are determined via the following thermodynamic condition:

$$\left. \frac{\partial p(v, T)}{\partial v} \right|_T = 0 \quad (31)$$

According to the Gibbs Phase Rule, spinodals have one degree of freedom in one-component systems: one component ($c = 1$) and one phase ($ph = 1$) from Eq. (30) yield $d = 2$ which has to be reduced by one due to the spinodal condition Eq. (31), which is an additional condition reducing the number of independent variables in Eq. (30) from two to one. Hence, one can first fix the temperature, T , and iterate the density to satisfy the above condition. Alternatively, one can iterate the temperature at constant density. Both methods yield the values of T and ρ , which can afterwards be substituted into an equation of state to calculate the spinodal pressure.

The calculation of critical points requires solving of two equations (which can alternatively be also expressed in terms of the density, ρ):

$$\left. \frac{\partial p(v, T)}{\partial v} \right|_T = \left. \frac{\partial^2 p(v, T)}{\partial v^2} \right|_T = 0 \quad (32)$$

From the Gibbs Phase Rule it follows that the critical point is invariant in one component systems, i.e. it has zero degree of freedom: $c = 1$, $ph = 1$ and two equations Eqs. (32) reducing the number of independent variables in Eq. (30) from two to zero yields $d = 0$. Therefore, both the temperature and the density must be iterated simultaneously in Eqs. (32). The critical pressure is calculated afterwards by substituting the results for T and ρ into the equation of state.

For the spinodal and critical point conditions Eqs. (31) and (32) one needs derivatives of the pressure with respect to the volume. In our work here, we obtained these derivatives analytically, which reduces the calculation error strongly, if compared to a numerical evaluation of the derivatives.

Eqs. (29), (31) and (32) are nonlinear equations, which preclude analytical evaluation of solutions. Different iteration solvers can be used for such problems, which however usually require initial (“guess”) values of the variables. In the case of one-root problems, such initial values can be taken far from an actual solution. However, if one deals with a many-root problem, a good choice of initial variables can be important. For example, if one would like to calculate the gas–liquid and liquid–liquid equilibria in binary mixtures or the corresponding critical curves, one cannot use only one set of initial parameters: These phenomena are usually separated from each other in the phase diagram and, therefore, one needs different initial parameters for solvers.

Similarly, one needs different initial parameters in order to calculate all types of critical points, phase equilibria and spinodals using the PC-SAFT model: gas–liquid-, “liquid–liquid”- and “gas–gas”-type of solutions exist there. There are different ways how to obtain such initial values. The simplest one is to scan, i.e. to calculate a series of isotherms to find out where they change the type from super- to subcritical and to use parameters in that vicinity for the iterative solver to calculate the solution exactly. There is also a more sophisticated method how to find out a new phenomenon in the phase diagram. This method is based on the fact that often there is a continuous transition between different critical/phase phenomena, if one changes the molecular parameters, e.g. the chain length parameter m

here or the energetic parameters ϵ_{ij} for mixtures, rather than the thermodynamic-state parameters. One can start, for example, from a known critical state and trace that solution beyond a boundary state which is usually a higher-order thermodynamic state such as a tricritical point (TCP) in mixtures. At a boundary state, a phenomenon changes its type, e.g. from a gas–liquid to a liquid–liquid type, and one obtains parameters for the new state. The continuity concept has been formulated for phase behavior in mixtures⁵⁹ and frequently applied to global phase diagram calculations^{60,61}.

Some misunderstanding can exist concerning the application of the Gibbs Phase Rule to the multiple critical points and the higher-order thermodynamic singularities, like double critical point and critical end point, discussed for one-component systems in this work. The Gibbs Phase Rule relating locally the thermodynamic states to the degree of freedom gives no information about the phase diagram topology globally. Since the critical points located in different parts of the phase diagram are not in equilibrium with each other, they comply with the Gibbs Phase Rule independently. The higher-order thermodynamic states should have a negative degree of freedom in experimental systems following the Gibbs Phase Rule. For example, for a one-component critical end point ($c = 1$) with two phases in equilibrium ($ph = 2$) and two critical-point conditions Eqs. (32) the Gibbs Phase Rule Eqs. (30) yields $d = -1$ for the degree of freedom. However, such states are also thermodynamically legitimate in theoretical investigations because an additional variable, i.e. the segment parameter m , can be included into the consideration increasing the number of independent variables in Eqn. (30) from two to three. The critical end point is invariant in this case, i.e. it can exist only for isolated (discrete) values of the chain length parameter m and the thermodynamic variables T , ρ and p . This discussion is also true for a double critical point, for which the thermodynamic relation is:

$$\left. \frac{\partial p(v, T)}{\partial v} \right|_T = \left. \frac{\partial^2 p(v, T)}{\partial v^2} \right|_T = \left. \frac{\partial^3 p(v, T)}{\partial v^3} \right|_T = 0 \quad (33)$$

The double critical point is a boundary state between the metastable and unstable critical states, which looks like a shoulder in a density-temperature diagram. One can compare a double critical point and a critical end point in one-component systems with a tricritical point in binary mixtures: It has the degree of freedom -1 in binary mixtures. However, including molecular parameters (ϵ_{ij}) in addition to the thermodynamic parameters in theoretical investigation makes the degree of freedom non-negative for the tricritical point. This

method of the phase diagram investigation is called global phase diagram method and used later on in this paper.

V. RESULTS

A. Phase Diagrams of Selected Systems

In the following part, the investigation of the phase diagram is reported for chain molecules with 29 beads per molecule and for monomers using the different levels of the PC-SAFT approach discussed above. The isotherms are compared to Monte Carlo simulations of the corresponding molecular model. In fact, the choice $m = 29$ is convenient for Monte Carlo studies (considerably longer chains would be difficult to equilibrate), and this choice of m is large enough, that properties for polymer melts are expected.

In Fig. 5 the phase diagram is shown which has been calculated using the PC-SAFT equation (level 3) for chain molecules with $m = 29$. The Monte Carlo simulations of the bead-spring chain molecules with $m = 29$ using both the NPT and NVT ensembles are also included in the figure. The simulations are performed for the same temperatures as the calculations with PC-SAFT (except $T_c^* = 0.768$).

The equation of state predicts two coexistence regions: the gas–liquid region at low density with reduced critical temperature $T_c^* = 3.868$ and reduced critical pressure $p_c^* = 0.00463$, and a “liquid–liquid” region at high density with reduced critical temperature $T_c^* = 0.768$ and reduced critical pressure $p_c^* = 5.66$. The reduced parameters are given in Lennard-Jones units.

The gas–liquid critical temperature in the simulations is much lower than the equation-of-state critical temperature, which is obvious from the shape of the isotherm at $T^* = 3$: It is a super-critical isotherm in the simulations, but it is a liquid-type isotherm in the analytical model. From the shape of the PC-SAFT isotherm at $T^* = 1$ one can see that the influence of the “liquid–liquid” demixing extends far into the region of the homogeneous liquid: The super-critical isotherm flattens out. This effect is very pronounced for $T^* = 1$; therefore, it can be expected for higher temperatures too.

In our Monte Carlo simulations of the coarse-grained bead-spring model for chain molecules carried out down to temperature $T^* = 0.75$ we could not find any evidence

of such “liquid–liquid” demixing. The pressure along the simulated isotherms increases monotonously in marked contrast to the PC-SAFT isotherms for $T^* < 1$.

At high pressure, the isotherms calculated with the analytical model exhibit a crossing. The possibility that such thermodynamic anomaly can occur in models employing a temperature-dependent co-volume or volume translation method⁶² widely used in the field of chemical engineering has previously been reported in the literature^{63,64,65,66}. This region however is not accessible to our Monte Carlo simulations.

Summarizing, the PC-SAFT equation exhibits unusual “liquid–liquid” demixing with a critical point and the crossing of isotherms at high density. Recently, Magee and Wilding⁶⁷ have reported a second critical point for the Lennard-Jones-Devonshire cell model – a basic cell model for the Lennard-Jones fluid. Furthermore, White⁶⁸ has studied an analytical model for the potential with repulsive shoulder and reported three critical points and closed-loop liquid–liquid equilibria for one-component systems. Hence, it is not for the first time that the analytical theories predict phase demixing which does not exist in the underlying molecular model. Our attempt to perform a quantitative comparison of the PC-SAFT model and the Monte Carlo simulations of the coarse-grained bead-spring model based on the Lennard-Jones+FENE potential does not yield good agreement for the same choice of molecular parameters. However, this disagreement might be due to inadequate representation of the molecular interactions implicitly captured by fitting the PC-SAFT equation to real substances. To investigate the source of these discrepancies we now compare computer simulations and corresponding analytical models.

In Fig. 6 the phase diagram for the CK-PC-SAFT equation and Monte Carlo simulations of the Chen-Kreglewski chain molecules are shown. This is precisely the same potential as modeled by the CK-PC-SAFT equation. One can see that the agreement between the equation of state and the simulations is much better in this case (e.g. for the high-temperature isotherms at $T^* = 10$ and $T^* = 4$ as well as for the low-temperature isotherms $T^* = 1$ and $T^* = 0.75$). However, the analytical calculations exhibit systematic deviations from the simulation results for a liquid-like density: For temperatures between $T^* = 3$ and $T^* = 1$, the density obtained from the simulations is somewhat lower than that from the equation-of-state calculations (i.e., for the same density the pressure from the simulations is higher than from the equation of state). At high ($T^* \geq 4$) and low ($T^* \approx 1$) temperatures, however, these deviations vanish. At low density and high temperature, the situation is opposite: The

pressure from the simulations is lower than from the model calculations.

A remarkably good agreement is obtained for $T^* = 3$ and $p^* = 0.05$ in the vicinity of the gas–liquid critical point. The equation-of-state critical point is at $T_c^* = 2.87$ and $p_c^* = 0.03$. Typically, one would expect rather poor agreement near a critical point, since it cannot be described by mean field theories correctly. The critical fluctuations can be accounted for by simulations, although they are restricted by the size of the simulation box. However, they are completely ignored in the equation-of-state models. A finite size scaling analysis can be applied to computer simulations in order to determine the critical point in the thermodynamic limit. Since we are interested in gross feature of the equation-of-state model, which can also be deduced from non-critical data, we set here aside the investigation of the finite size analysis near the critical points. The reason for this perfect agreement becomes clear if one analyzes another systematic deviation between the simulations and the equation-of-state calculations for isotherms $T^* = 4$ and $T^* = 10$: The simulation results are above the calculated curves at high pressure and are below these curves at low pressure. Therefore, there is a pressure at which both methods yield similar results. For $T^* = 10$, this pressure is about $p^* \approx 1$, and for $T^* = 4$ it is $p^* \approx 0.2$ (see Fig. 6). For $T^* = 3$, the same result is obtained at $p^* = 0.05$.

The “liquid–liquid” demixing found with PC-SAFT is also predicted by CK-PC-SAFT, albeit at lower temperature: The “liquid–liquid” critical point is located at $T^* = 0.2$. The direct investigation of this region using Monte Carlo simulations is not possible, since the chain molecules exhibit a glass transition at high density ($\rho > 1$), and the equilibration of chains slows down very rapidly. Therefore, we base our investigation on the further systematic analysis of the model hierarchy. Moreover, the CK-PC-SAFT equation exhibits a crossing of the isotherms at high pressure similar to the PC-SAFT equation. A comparison of the simulation results to the analytical calculations for $T^* = 4$ and $T^* = 10$ again shows a systematic deviation as pressure increases, which is related to this crossing of the isotherms.

Summarizing, the CK-PC-SAFT equation predicts the same topology of the phase diagram as the PC-SAFT equation with $m = 29$: One finds the crossing of the isotherms and the “liquid–liquid” phase separation at high density but at much lower temperatures than in PC-SAFT. The replacement of the PC-SAFT dispersion by the square-well dispersion cannot correct these artifacts.

In the next step, we remove the approximation of the “softened” repulsion, modeled by the

effective, temperature-dependent diameter $d(T)$, which turns the Chen–Kreglewski potential into the square-well potential. In Fig. 7 the phase diagram for square-well chains with 29 beads/molecule obtained using the SW-PC-SAFT equation and Monte Carlo simulations of isotherms for precisely the same potential are shown. One can observe that the removal of the effective-diameter approximation avoids the crossing of the isotherms at high pressure and improves the overall agreement between the equation-of-state calculations and Monte Carlo simulations. Therefore, one can trace back the crossing of the isotherms and the inaccuracy of the CK-PC-SAFT equation at liquid density to the temperature-dependent diameter.

The critical temperature and the phase envelope of the “liquid–liquid” demixing are nearly identical for SW-PC-SAFT and CK-PC-SAFT, because at low temperature the effective diameter, $d(T)$, approaches the hard-sphere diameter, σ (see Fig. 2). In fact, the value of $u(r)/k_{\text{B}}T$ calculated from the potential energy, $u(r)$, for the Chen-Kreglewski “softened” repulsion diverges at low temperature and in the low-temperature limit it turns to be the same as for the square-well potential (i.e. infinity).

Theoretical considerations suggest that liquid–liquid phase coexistence can occur in systems with softened potentials⁶⁹ and this behavior was recently investigated in computer simulations^{70,71}. However, the “liquid–liquid” demixing found with PC-SAFT and CK-PC-SAFT here is also present in the square-well equation for chains (SW-PC-SAFT) – a model which does not include the “softened” repulsion, and where the “liquid–liquid” demixing clearly is not expected. Hence, one can conclude that the “liquid–liquid” demixing predicted by these equations of state is due to inappropriate approximations in the dispersion term and does not reflect the statistical mechanics of the model.

By setting $m = 1$, one can reduce the PC-SAFT model of chain molecules to monomers. In this case, the chain term in equation Eq.(3) vanishes and the reference hard-chain fluid turns into the hard-sphere fluid. The m dependencies in the dispersion term vanish too, and the set of universal constants (a_{ij} and b_{ij} with $i = 0, 1, 2$ and $j = 0..6$) for Eqs. (21) and (22) reduces from 42 to 14 constants (a_{0j} and b_{0j}). In Fig. 8 the compressibility factor is shown as function of the packing fraction calculated from the SW-PC-SAFT equation for monomers. At high temperatures, the analytical results are in excellent agreement with the simulations. The gas–liquid demixing occurs at low density and high temperature. At low temperature and high density, the SW-PC-SAFT equation for monomers predicts a “liquid–

liquid” demixing with critical temperature $T_c^* = 0.296$. However, this phase coexistence is not expected for the square-well potential.

The PC-SAFT approach for a one-component system of monomers thus exhibits unusual “liquid–liquid” phase separation phenomena, which persists further for chain molecules. This demixing is not related to the modeling of the “softened” repulsion, since this repulsion is not present in the square-well potential, but rather to the use of approximations for the dispersion term, e.g. a power series with fitted coefficients. A related problem due to a power series expansion of dispersion terms has already been reported in the literature⁷². In order to investigate this problematic feature of the model systematically, we perform global calculations of the phase behavior including the polymer-like long chain molecules in our study.

B. Global Phase Behavior

For a systematic classification of the phase diagrams predicted with the van der Waals equation of state for mixtures, van Konynenburg and Scott^{73,74} have proposed a method which is called global phase diagram method^{75,76}. This method is based on grouping the binary phase diagrams according to a topological similarity of the phase equilibrium surface in the space of the reduced molecular (energetic and geometric) parameters. In binary mixtures, for example, there are two sets of the molecular parameters for each component, $(\epsilon_{11}, \sigma_{11})$ and $(\epsilon_{22}, \sigma_{22})$, and one set of the cross-interaction parameters, $(\epsilon_{12}, \sigma_{12})$, which are also called binary parameters. The different types of the phase behavior are separated in the molecular parameter space by the boundaries representing the higher order thermodynamic states such as a tricritical point (TCP) and a double critical end point (DCEP). The global phase diagram method has already been applied to many equations of state, binary and ternary systems, polar and polymeric substances^{60,77,78,79,80,81,82,83,84,85,86,87}.

In a one-component chain fluid, the effective chain interactions of an entire chain change for different chain lengths. Thus, in contrast to simple molecules, there is a variety of one-component phase diagrams for different m values and fixed segment interaction parameters, ϵ and σ . For real substances, e.g., the homologous series of alkanes, these phase diagrams are qualitatively similar; however, they differ by the location in the thermodynamic parameter space: The coexistence curve and critical point typically shift to lower pressure and density

and to higher temperature for long chains. Within the PC-SAFT approach one can define a common set of segment interaction parameters, ϵ and σ , which is independent of m , and study the topology of the phase diagrams for different chain lengths.

In Fig. 9 the temperature-packing fraction phase diagram of one-component chains calculated using the PC-SAFT equation is shown. The chain length parameters included in these calculations are $m = 1$ and $m = 100$. In addition to the physically reasonable gas-liquid-type critical point, a “liquid-liquid”-type demixing is found for all values of m in these calculations. As m increases, the “liquid-liquid”-type phase separation shifts to lower packing fraction $\eta \approx 0.52$ and higher temperature $T^* \approx 0.8$, a region of temperature and density which is of experimental interest for macromolecules. Furthermore, a “gas-liquid-liquid”-type phase coexistence can occur within the model. For monomers, this three-phase equilibrium is found at low temperature and vanishing pressure; for long chains the temperature increases to $T^* \approx 0.7$. The shape of the gas-liquid coexistence curve (and spinodals) can hence be affected by these three-phase equilibria due to the thermodynamic relations for the coexisting phases. For example, the location of the phase in the middle (at $\eta \approx 0.5$) and the shape of the binodal are defined not only by the gas phase at low density, but also by the second “liquid” phase at high density.

A “gas-gas”-type critical point can be found for PC-SAFT in the low-density region of the phase diagram at packing fraction $\eta < 10^{-2}$ and chain length parameter $m \geq 70$. An enlargement of this region is shown in Fig. 10 for chain lengths $m = 1, 70, 100, 1000$. An additional critical point at low density appears for chain length $m \approx 70$, indicated in Fig. 10 by a shoulder on the left side of the gas-liquid spinodal for $m = 70$. For a larger m , this “gas-gas” critical point touches the binodal, which yields first a critical end point (CEP), and then a “gas-gas-liquid” coexistence with two stable critical points in the gas-liquid region of the phase diagram. As an example, the case $m = 100$ is shown in Fig. 10. For these and longer chains (e.g., $m = 1000$ representing the polymer limit in the figure), this new critical point affects the shape of spinodal and coexistence curves. Thus, the PC-SAFT equation erroneously describes the low density behavior, where one would expect a nearly ideal-gas behavior.

A global investigation of the pressure-temperature phase diagrams calculated with PC-SAFT is shown in Fig. 11 and explained schematically in Fig. 12. For large m , the gas-liquid critical point can move to negative pressure in PC-SAFT. Usually, it is not possible that the

gas phase coexists at negative pressure. In contrast, liquids can exhibit a phase coexistence and critical phenomena in a metastable state at negative pressure^{88,89}. The PC-SAFT model predicts a “gas–gas” demixing with a critical point for $m \geq 70$ as has been shown above. For $m \approx 70$, a double critical point appears on the gaseous spinodal, which causes a cusp of the otherwise smooth spinodal curve (Fig. 11 and inset 2 in Fig. 12). This double critical point yields two new critical points: one metastable “gas–gas” critical point and one unstable critical point, which looks like a shoulder on the spinodal curve in the temperature–packing fraction diagram in Fig. 10.

For m slightly larger than 70, the metastable “gas–gas” critical point touches the binodal curve in a critical end point (CEP) (inset 3 in Fig. 12). For $m = 100$, two stable critical points for the “gas–gas”- and gas–liquid-type demixing exist in the diagram as well as the “gas–gas–liquid”-type triple point with three binodal curves in the vicinity (inset 4 in Fig. 12 and Fig. 10). Further increase of m causes the gas–liquid critical point to shift to lower pressure until it touches the binodal curve in a second critical end point (CEP) (inset 5 in Fig. 12). Beyond this CEP the gas–liquid critical point becomes metastable and can shift to negative pressure, e.g. for the case $m = 1000$ shown in Fig. 11 and inset 6 in Fig. 12. The new “gas–gas” critical point changes its type to a gas–liquid critical point after passing the critical end point and takes the place of the “former” gas–liquid critical point. Such multiple critical phenomena and transformations are well known from the investigations of the tricritical points in binary fluid mixtures. Here, however, they are found using the PC-SAFT equation for one-component systems.

In contrast, the “liquid–liquid” demixing and the “liquid–liquid” critical point exist at physical pressure and temperature for all values of the chain parameter m . The “liquid–liquid” critical pressure decreases slightly with increasing chain length parameter m and converges to a constant value $p_c^* \approx 5.194$ (in Lennard-Jones units) for infinitely long polymers. The “liquid–liquid” critical temperature converges to $T_c^* \approx 0.796$ and the coexistence region shifts to higher temperature.

C. Application to Correlations of Polybutadiene Data

In order to investigate the impact of the artificial phase separations discussed above on applications of practical interest, the PC-SAFT equation is applied to experimental data

of polybutadiene with molecular mass $M_w = 45000$ g/mol provided by BASF Aktiengesellschaft. Experimental data for the density of polybutadiene at various pressures and correlations with the PC-SAFT model using two molecular parameter sets are shown in Figure 13. The parameter set 1 with $m = 1800$ gives a very good representation of the liquid density at high temperature. Some discrepancies can be found at low temperature for high pressure isobars. The parameter set 2 with $m = 1098$ gives worse correlation of the experimental data. At high pressure, these discrepancies are very large (note that the solid curve denotes $p = 200$ MPa and the dashed curve corresponds to $p = 100$ MPa in Fig. 13). The calculated isobars splay out at low temperature unlike the experimental isobars which can be approximated with straight lines in this temperature region fairly well. Furthermore, the splay of the calculated isobars is stronger at higher pressure (compare isobars 200 MPa and 0.1 MPa in Fig. 13).

In Fig. 14 the data are correlated by a new set of parameters, which yields the best possible representation of the experimental data. A comparison between the isobars for the lowest and the highest pressures reveals that the density variation decreases by about 30% in that temperature range, i.e., the temperature dependence of the isobaric density becomes weaker for polybutadiene at high pressure. This can be deduced from the experimental data which approach each other at high pressure. For the PC-SAFT model, however, the distance between the isotherms increases at high density. This problem is caused by the unusual “liquid–liquid” phase separation region in PC-SAFT for the parameters supposed to describe polybutadiene shown in Fig. 14.

The flattening of the critical isotherm at the “liquid–liquid” critical point ($T_c = 214$ K, $p_c = 492$ MPa) leads to deviations from the actual behavior already for isotherms at much higher temperatures and much lower pressures, since pressure effects to this transition set in very gradually. Therefore, this artifact of the PC-SAFT approach has a direct influence on the correlation of the data for polybutadiene and excludes any valid extrapolation of the polybutadiene behavior outside the experimentally measured range.

VI. CONCLUSIONS

The phase diagram of the Perturbed-Chain Statistical Associating Fluid Theory (PC-SAFT) has been studied for a wide range of the chain length parameter m and thermody-

dynamic parameters such as temperature, pressure and density. For a systematic investigation, a hierarchy of the models, which can be derived from the PC-SAFT approach to chain molecules, has been analyzed and compared to Monte Carlo simulations of the square-well potential, the Chen-Kreglewski potential, and a coarse-grained bead-spring model of chain molecules. The aim of this study was to test the ability of such PC-SAFT based approaches to accurately predict equation of state properties of polymers. Unfortunately, we have found that this approach suffers from artificial “gas–gas” and “liquid–liquid” demixing phenomena.

The PC-SAFT equation predicts a “gas–gas” critical demixing at low densities and a “liquid–liquid” critical demixing at high densities in addition to the common gas–liquid demixing. These critical phenomena and phase equilibria exist usually in mixtures, however, within this theory they have been found for one-component fluids. Based on a systematic analysis of a hierarchy of the PC-SAFT approach it is shown that the “liquid–liquid” demixing is not due to the “softened” repulsion, but rather caused by approximations in the dispersion term of the equation of state. In the following we summarize this rather unusual behavior.

The “gas–gas” critical point appears on the gaseous side of the gas–liquid spinodal for the chain length parameter $m \approx 70$ and persists for larger m . Therefore, in the low-density part of the phase diagram, one can find at high temperature two critical points for the “gas–gas” and gas–liquid demixing, three-phase equilibria (“gas–gas–liquid”), and two critical end points (a gaseous critical phase in equilibrium with a liquid phase and a gas phase in equilibrium with a gas–liquid-type critical phase). For $m > 210$, the gas–liquid critical point shifts to negative pressure and the “gas–gas” critical point becomes the gas–liquid critical point. This transformation of the critical point affects the shape of the coexistence curve.

The “liquid–liquid” phase separation has been found at high density and low temperature where usually a solid–liquid phase transition or a glass transition in polymers can be expected. At high pressure, this “liquid–liquid” demixing exhibits a critical point for all values of the chain length parameter m . The location of the “liquid–liquid”-type critical point and the “liquid–liquid” immiscibility region in the phase diagram depends on the chain length parameter. For long chains, the “liquid–liquid” demixing shifts to higher temperature and lower pressure. In the limit of infinitely long chains, the parameters of the “liquid–liquid” critical point approach finite values for the reduced critical pressure $p_c^* \approx 5.194$ and the reduced critical temperature $T_c^* \approx 0.796$ (in Lennard-Jones units). These values correspond

to about $p_c \approx 280$ MPa and $T_c \approx 200$ K for typical values of the Lennard-Jones parameters $\epsilon/k_B = 250$ K and $\sigma = 4$ Å.

The thermodynamic state parameters that correspond to the “gas–gas” and “liquid–liquid” coexistence regions are quite remote from those in typical experiments with low and moderate molecular weight polymers. Therefore at first sight one might expect that in the region of experimental interest these artificial phase separation phenomena, that do not correspond to any physical behavior of the system, do not matter much.

However, for a polybutadiene melt, for example, it has been shown here that the ability of the PC-SAFT equation to correlate the density of macromolecular substances is affected by the region of “liquid–liquid” demixing. The immiscibility region in this case is located at the packing fraction $\eta \geq 0.51$, whereas the experimental polybutadiene data are in the range of the packing fractions $0.44 \leq \eta \leq 0.49$. However, the “liquid–liquid” demixing extends its influence on the thermodynamic properties of a homogeneous fluid far into the experimentally relevant region of the state parameters. We recall that mean field theory predicts a Curie–Weiss-type divergence of the compressibility $\kappa \propto 1/(T - T_c)$ at the critical point (with T_c being the critical temperature) and, therefore, the compressibility is significantly enhanced over a wide region in the temperature-density diagram in the vicinity of the critical point.

Furthermore, the continuity concept formulated for phase behavior of mixtures⁵⁹ if applied to one-component systems means that a phase phenomenon existing in one region of the phase diagram affects also neighboring regions. For example, an isotherm can change the slope because of a spinodal or a critical point in its vicinity; a coexistence curve can exhibit a shoulder due to a metastable critical point in the vicinity of a critical end point (CEP). Furthermore, a wrong location of a spinodal can predict the phase separation kinetics incorrectly. For caloric properties and expansion coefficients one can expect large deviations or even divergence-like anomalies in the vicinity of the unusual immiscibility regions since these quantities are related to derivatives, e.g. the isobaric thermal expansion $\alpha_P = V^{-1}(\partial V/\partial T)_P$ or the isothermal compressibility $K_T = -V^{-1}(\partial V/\partial p)_T$.

The impact of the unusual phase behavior is also important when the model is applied to high molecular weight polymers and mixtures, e.g. polymer solutions or polymer blends. The mixing rules employed usually for modeling mixtures can cause the critical points to shift into the experimentally relevant region of thermodynamic parameters, especially for

systems with large differences between the critical parameters^{90,91}. For polymers in such cases, one speaks about a hypothetical critical point, which is related to the chain length parameter m and the molecular parameters ϵ and σ . It is *a priori* not clear whether this unusual phase separation moves closer to the parameter region of physical interest, when a solvent is added, or whether it moves further away. It seems plausible that the answer to this question will not be universal, but will rather depend on the nature of the solvent. These facts have to be considered utilizing PC-SAFT models to predict thermodynamic properties, e.g. extrapolations into regions which cannot be fitted to the equation of state parameters due to the lack of experimental data but which are of practical interest to investigate.

VII. ACKNOWLEDGMENTS

This work was supported by BASF Aktiengesellschaft (Ludwigshafen, Germany). We benefited from stimulating discussions with H. Weiss, U. Nieken, W. Hültenschmidt, Ch. Ch. Liew, A. Moreira, O. Evers (BASF Aktiengesellschaft, Ludwigshafen). We are also grateful to the BASF Aktiengesellschaft for supplying the thermodynamic data on polybutadiene shown in Figs. 13 and 14 as well as the equation parameters and the calculations shown in Fig. 13. We thank P. Virnau (MIT, Cambridge) for interesting discussions and for providing us with the Monte Carlo LJ+FENE code as well as L. G. MacDowell (Madrid, Spain) for his fruitful collaboration. CPU time was provided by the computing center of the Johannes-Gutenberg University of Mainz.

-
- ¹ P. J. Flory, *Principles of Polymer Chemistry* (Cornell University Press: Ithaca, NY, 1953).
 - ² I. C. Sanchez and R. H. Lacombe, *Macromolecules* **11**, 1145 (1978).
 - ³ I. C. Sanchez and R. H. Lacombe, *Polymer* **36**, 2929 (1995).
 - ⁴ M. S. Wertheim, *J. Stat. Phys.* **35**, 19 (1984).
 - ⁵ M. S. Wertheim, *J. Stat. Phys.* **35**, 35 (1984).
 - ⁶ M. S. Wertheim, *J. Stat. Phys.* **42**, 459 (1986).
 - ⁷ M. S. Wertheim, *J. Stat. Phys.* **42**, 477 (1986).
 - ⁸ M. S. Wertheim, *J. Chem. Phys.* **85**, 2929 (1986).
 - ⁹ M. S. Wertheim, *J. Chem. Phys.* **87**, 7323 (1987).
 - ¹⁰ G. Jackson, W. G. Chapman, and K. E. Gubbins, *Mol. Phys.* **65**, 1 (1988).
 - ¹¹ W. G. Chapman, G. Jackson, and K. E. Gubbins, *Mol. Phys.* **65**, 1057 (1988).
 - ¹² R. W. Zwanzig, *J. Chem. Phys.* **22**, 1420 (1954).
 - ¹³ J. A. Barker and D. Henderson, *J. Chem. Phys.* **47**, 2856 (1967).
 - ¹⁴ J. A. Barker and D. Henderson, *J. Chem. Phys.* **47**, 4714 (1967).
 - ¹⁵ J. D. Weeks, D. Chandler, and H. C. Andersen, *J. Chem. Phys.* **71**, 5237 (1971).
 - ¹⁶ W. G. Chapman, K. E. Gubbins, G. Jackson, and M. Radosz, *Fluid Phase Equilibria* **52**, 31 (1989).
 - ¹⁷ W. G. Chapman, K. E. Gubbins, G. Jackson, and M. Radosz, *Ind. Eng. Chem. Res.* **29**, 1709 (1990).
 - ¹⁸ E. A. Müller and K. E. Gubbins, *Ind. Eng. Chem. Res.* **40**, 2198 (2001).
 - ¹⁹ I. G. Economou, *Ind. Eng. Chem. Res.* **41**, 953 (2002).
 - ²⁰ A. Gil-Villegas, A. Galindo, P. J. Whitehead, S. J. Mills, G. Jackson, and A. N. Burgess, *J. Chem. Phys.* **106**, 4168 (1997).
 - ²¹ A. Galindo, L. A. Davies, A. Gil-Villegas, and G. Jackson, *Mol. Phys.* **93**, 241 (1998).
 - ²² T. Kraska and K. E. Gubbins, *Ind. Eng. Chem. Res.* **35**, 4727 (1996).
 - ²³ F. J. Blas and L. F. Vega, *Mol. Phys.* **92**, 135 (1997).
 - ²⁴ F. J. Blas and L. F. Vega, *Ind. Eng. Chem. Res.* **37**, 660 (1998).
 - ²⁵ L. G. MacDowell, M. Müller, C. Vega, and K. Binder, *J. Chem. Phys.* **113**, 419 (2000).
 - ²⁶ L. G. MacDowell, P. Virnau, M. Müller, and K. Binder, *J. Chem. Phys.* **117**, 6360 (2002).

- ²⁷ J. Gross, Dissertation, TU Berlin (2001).
- ²⁸ J. Gross and G. Sadowski, *Ind. Eng. Chem. Res.* **40**, 1244 (2001).
- ²⁹ J. Gross and G. Sadowski, *Ind. Eng. Chem. Res.* **41**, 1084 (2002).
- ³⁰ J. Gross, O. Spuhl, F. Tumakaka, and G. Sadowski, *Ind. Eng. Chem. Res.* **42**, 1266 (2003).
- ³¹ J. Vijande, M. M. Piñeiro, D. Bessires, H. Saint-Guirons, and J. L. Legid, *Phys. Chem. Chem. Phys.* **4**, 766 (2004).
- ³² E. L. Cheluget, C. P. Bokis, L. Wardhaugh, C.-C. Chen, and J. Fisher, *Ind. Eng. Chem. Res.* **41**, 968 (2002).
- ³³ S. E. Quiñones Cisneros, *Phys. Chem. Chem. Phys.* **6**, 2307 (2004).
- ³⁴ O. Spuhl, S. Herzog, J. Gross, I. Smirnova, and W. Arlt, *Ind. Eng. Chem. Res.* **43**, 4457 (2004).
- ³⁵ N. von Solms, M. L. Michelsen, and G. M. Kontogeorgis, *Ind. Eng. Chem. Res.* **42**, 1098 (2003).
- ³⁶ N. F. Carnahan and K. E. Starling, *J. Chem. Phys.* **51**, 635 (1969).
- ³⁷ T. Boublík, *J. Chem. Phys.* **53**, 471 (1970).
- ³⁸ G. A. Mansoori, N. F. Carnahan, K. E. Starling, and L. T. W., *J. Chem. Phys.* **54**, 1523 (1971).
- ³⁹ B. J. Alder, D. A. Young, and M. A. Mark, *J. Chem. Phys.* **56**, 3013 (1972).
- ⁴⁰ Y. G. Chiew, *J. Chem. Phys.* **93**, 5067 (1990).
- ⁴¹ Y. G. Chiew, *Mol. Phys.* **73**, 359 (1991).
- ⁴² Y. Tang and B. C.-Y. Lu, *J. Chem. Phys.* **105**, 8262 (1996).
- ⁴³ J. Chang and H. Kim, *J. Chem. Phys.* **109**, 2579 (1998).
- ⁴⁴ J. Chang and H. Kim, *Mol. Phys.* **96**, 1789 (1999).
- ⁴⁵ H. S. Gulati and C. K. Hall, *J. Chem. Phys.* **107**, 3930 (1997).
- ⁴⁶ T. Hino and J. M. Prausnitz, *Fluid Phase Equilibria* **138**, 105 (1997).
- ⁴⁷ J. Gross and G. Sadowski, *Fluid Phase Equilibria* **168**, 183 (2000).
- ⁴⁸ K. Binder, M. Müller, P. Virnau, and L. G. MacDowell, *Adv. Polym. Sci.* **173**, 1 (2005).
- ⁴⁹ P. Virnau, M. Müller, L. G. MacDowell, and K. Binder, *J. Chem. Phys.* **121**, 2169 (2004).
- ⁵⁰ S. S. Chen and A. Kreglewski, *Ber. Bunsen-Ges.* **81**, 1048 (1977).
- ⁵¹ S. H. Huang and M. Radosz, *Ind. Eng. Chem. Res.* **29**, 2284 (1990).
- ⁵² K. Kremer and G. S. Grest, *J. Chem. Phys.* **92**, 5057 (1990).
- ⁵³ P. Virnau, M. Müller, L. G. MacDowell, and K. Binder, *Comp. Phys. Comm.* **147**, 378 (2002).
- ⁵⁴ B. Smit, *J. Chem. Phys.* **96**, 8639 (1992).
- ⁵⁵ P. Virnau, Dissertation, Universität Mainz (2003).

- ⁵⁶ D. Frenkel and B. Smit, *Understanding Molecular Simulation: From Algorithms to Applications* (Academic Press, 2002).
- ⁵⁷ G. D. Smith, W. Paul, M. Monkenbusch, L. Willner, D. Richter, X. H. Qiu, and M. D. Ediger, *Macromolecules* **32**, 8857 (1999).
- ⁵⁸ S. Krushev, Dissertation, Universität Mainz (2002).
- ⁵⁹ G. M. Schneider, *Phys. Chem. Chem. Phys.* **6**, 2285 (2004).
- ⁶⁰ L. V. Yelash and T. Kraska, *Ber. Bunsenges. Phys. Chem.* **102**, 213 (1998).
- ⁶¹ L. V. Yelash and T. Kraska, *Z. für Phys. Chemie* **211**, 159 (1999).
- ⁶² J. J. Martin, *Ind. Eng. Chem. Fundam.* **18**, 81 (1979).
- ⁶³ P. H. Salim and M. A. Trebble, *Fluid Phase Equilibria* **65**, 59 (1991).
- ⁶⁴ O. Pfohl, *Fluid Phase Equilibria* **163**, 157 (1999).
- ⁶⁵ I. Polishuk, J. Wishnjak, H. Segura, L. V. Yelash, and T. Kraska, *Fluid Phase Equilibria* **172**, 1 (2000).
- ⁶⁶ L. V. Yelash and T. Kraska, *AIChE J.* **49**, 1569 (2003).
- ⁶⁷ J. E. Magee and N. B. Wilding, *Mol. Phys.* **100**, 1641 (2002).
- ⁶⁸ J. A. White, *Physika A* **346**, 347 (2005).
- ⁶⁹ G. Stell and P. C. Hemmer, *J. Chem. Phys.* **56**, 4274 (1972).
- ⁷⁰ E. A. Jagla, *Phys. Rev. E* **63**, 061501 (2001).
- ⁷¹ B. Pellicane, G. Pellicane, and G. Malescio, *J. Chem. Phys.* **120**, 8671 (2004).
- ⁷² N. Koak, T. W. de Loos, and R. A. Heidemann, *Ind. Eng. Chem. Res.* **38**, 1718 (1999).
- ⁷³ R. L. Scott and P. H. van Konynenburg, *Discuss. Faraday Soc.* **49**, 87 (1970).
- ⁷⁴ P. H. van Konynenburg and R. L. Scott, *Philos. Trans. Roy. Soc. London* **248A**, 495 (1980).
- ⁷⁵ D. Furman and R. B. Griffiths, *Phys. Rev. A* **17**, 1139 (1978).
- ⁷⁶ D. Furman, S. Dattagupta, and R. B. Griffiths, *Phys. Rev. B* **15**, 441 (1978).
- ⁷⁷ U. K. Deiters and I. L. Pegg, *J. Chem. Phys.* **90**, 6632 (1989).
- ⁷⁸ A. van Pelt, C. J. Peters, and J. de Swaan Arons, *J. Chem. Phys.* **95**, 7569 (1991).
- ⁷⁹ T. Kraska and U. K. Deiters, *J. Chem. Phys.* **96**, 539 (1992).
- ⁸⁰ M. Bluma and U. K. Deiters, *Phys. Chem. Chem. Phys.* **1**, 4307 (1999).
- ⁸¹ T. Kraska, *Ber. Bunsenges. Phys. Chem.* **100**, 1318 (1996).
- ⁸² J. Kolafa, I. Nezbeda, J. Pavlíček, and W. R. Smith, *Fluid Phase Equilibria* **146**, 103 (1998).
- ⁸³ I. Nezbeda, J. Pavlíček, J. Kolafa, A. Galindo, and G. Jackson, *Fluid Phase Equilibria* **158–160**,

193 (1999).

- ⁸⁴ L. V. Yelash and T. Kraska, *Phys. Chem. Chem. Phys.* **1**, 4315 (1999).
- ⁸⁵ J.-L. Wang, G.-W. Wu, and R. J. Sadus, *Mol. Phys.* **98**, 715 (2000).
- ⁸⁶ R. L. Scott, *Phys. Chem. Chem. Phys.* **1**, 4225 (1999).
- ⁸⁷ L. V. Yelash, T. Kraska, and U. K. Deiters, *J. Chem. Phys.* **110**, 3079 (1999).
- ⁸⁸ A. R. Imre, T. Kraska, and L. V. Yelash, *Phys. Chem. Chem. Phys.* **4**, 992 (2002).
- ⁸⁹ A. Drozd-Rzoska, S. J. Rzoska, and A. R. Imre, *Phys. Chem. Chem. Phys.* **6**, 2291 (2004).
- ⁹⁰ J. Wishnjak, H. Segura, I. Polishuk, and T. Kraska, *Ind. Eng. Chem. Res.* **41**, 4414 (2002).
- ⁹¹ H. Segura, T. Kraska, J. Wishnjak, A. Mejía, and I. Polishuk, *Ind. Eng. Chem. Res.* **42**, 5662 (2003).

- Fig. 1** The interaction potential of Chen and Kreglewski⁵⁰. The solid circles represent the segment diameter σ . At that distance, the molecules repel each other with interaction energy equal to $+3\epsilon$. The interaction energy diverges at distance $r = 0.88\sigma$ (dashed circles). For comparison, the interaction energy in the hard-sphere and square-well models diverges at distance $r = \sigma$. The areas between the solid circles and the dotted circles correspond to the attraction well of the potential with energy depth $-\epsilon$. The corresponding potential curve is shown on the right hand side.
- Fig. 2** Temperature-dependent diameter calculated by applying the Barker-Henderson relation for the effective diameter to the Chen-Kreglewski potential. The hard-sphere diameter σ is recovered at low temperature. In the high-temperature limit, the effective diameter is $d(T) = 0.88\sigma$. $T^* = k_B T / \epsilon$ is the reduced temperature.
- Fig. 3** Bead-spring model for chain molecules. Circles represent the coarse-grained monomers. Springs represent the interactions between the bonded monomers, which interact via the Lennard-Jones+FENE potential. Non-bonded monomers interact via the Lennard-Jones potential. The corresponding potential curves are shown schematically on the right hand side.
- Fig. 4** Approximation of the Lennard-Jones potential by the Chen-Kreglewski potential with the same depth ϵ of the attraction well and the segment diameter σ .
- Fig. 5** Phase diagram and isotherms calculated for chain molecules with $m = 29$ beads per chain using the PC-SAFT equation (curves). The equation-of-state model exhibits a gas-liquid demixing at low density and a coexistence of two dense phases, which is called “liquid-liquid” demixing here. The gas-liquid-type reduced critical temperature and pressure are $T_c^* = 3.868$ and $p_c^* = 0.00463$, respectively. The “liquid-liquid”-type reduced critical temperature and pressure are $T_c^* = 0.768$ and $p_c^* = 5.66$, respectively. Bold curves are the coexistence regions; thin solid curves are the calculated isotherms for different temperatures; dashed curves are the critical isotherms. Monte Carlo simulations of the Lennard-Jones+FENE chains with $m = 29$ monomers per molecule (symbols) are shown for the same temperatures as the isotherms calculated with the equation of state (except $T_c^* = 0.768$). Error bars show the standard deviation for the density ob-

tained in NPT simulations and for the pressure obtained in NVT simulations. Dotted lines are guides to the eye for the Monte Carlo isotherms. Reduced pressure, temperature, and monomer density are given in the Lennard-Jones units: $p^* \equiv p\sigma^3/\epsilon$, $T^* \equiv k_B T/\epsilon$, and $\rho^* \equiv \rho\sigma^3$. The graph b) shows the vicinity of the “liquid–liquid” demixing predicted by the equation of state. Note that the isotherms in the simulations (symbols) have a different curvature as the subcritical ones in the analytical model (curves).

Fig. 6 Phase diagram and isotherms calculated with the CK-PC-SAFT equation (curves) and Monte Carlo simulations of isotherms (symbols) for the Chen-Kreglewski chain molecules with $m = 29$ monomers per molecule. The temperatures for the calculations and the simulations are $T^* = 10/4/3/2.87/2/1.6/1.4/1.2/1/0.75$. $T_c^* = 2.87$ is the gas–liquid critical isotherm from CK-PC-SAFT. The “liquid–liquid” critical isotherm ($T_c^* = 0.2$) and one sub-critical isotherm ($T^* = 0.16$) calculated with the CK-PC-SAFT equation are also shown. Dotted lines are guides to the eye for the simulated isotherms. Reduced parameters are defined as in Fig. 5.

Fig. 7 Phase diagram and isotherms calculated with the SW-PC-SAFT equation (curves) and Monte Carlo simulations of isotherms (symbols) for the square-well chains with 29 beads/molecule. The calculated and simulated temperatures are $T^* = 4/3/2.5/2/1/0.75$. $T_c^* = 2.5$ is the equation-of-state gas–liquid critical temperature. The “liquid–liquid” critical isotherm ($T_c^* = 0.2$) and one sub-critical isotherm for the “liquid–liquid” region ($T^* = 0.16$) calculated with the SW-PC-SAFT equation are also shown. In SW-PC-SAFT, the segment diameter is temperature-independent in contrast to the CK-PC-SAFT equation shown in Fig. 6. Dotted lines are guides to the eye for the simulated isotherms. Reduced parameters are defined as in Fig. 5.

Fig. 8 Packing-fraction dependence of the compressibility factor calculated with the SW-PC-SAFT equation for monomers ($m = 1$) for the reduced temperatures $T^* = 3, 2, 1.5, 0.75$, and 0.296 . The isotherm $T_c^* = 0.296$ is the critical isotherm for the “liquid–liquid” phase separation at high density. The gas–liquid demixing exists at low packing fraction and higher temperature. Symbols are Monte Carlo

simulations of the square-well monomers. Reduced temperature is defined as in Fig. 5.

- Fig. 9** A temperature–packing fraction phase diagram of one-component systems calculated using the PC-SAFT equation for monomers ($m = 1$) as well as for chain molecules with the chain length parameter $m=100$. Solid curves denote binodals; dashed curves correspond to spinodals. Dotted arrows show the trajectories of the gas–liquid and “liquid–liquid” critical points for different values of the chain length parameter m . The reduced temperature is $T^* = k_B T / \epsilon$; the packing fraction is $\eta = (\pi/6) \rho m d^3$.
- Fig. 10** Enlarged low-density region of the phase diagram in Fig. 9 showing “gas–gas” and “gas–gas–liquid” equilibria. The values of m are the numbers of repeat units per chain molecule. Legend for curves as in Fig. 9.
- Fig. 11** A one-component global phase diagram in pressure–temperature coordinates calculated with the PC-SAFT equation for different values of the chain length parameter m . Dash-dotted curves are the gas–liquid and “liquid–liquid” binodals for the monomer; bold curve is the “liquid–liquid” binodal for a polymer; solid thin curves are spinodals. Open circles are the gas–liquid and “gas–gas” critical points; filled circles are “liquid–liquid” critical points of monomer and polymer. Dotted curves show the trajectories of the gas–liquid, “gas–gas” and “liquid–liquid” critical points calculated for different values of the chain length parameter m .
- Fig. 12** Schematic explanation of the phase diagram topology in the pressure–temperature plane calculated in Fig. 11 using the PC-SAFT equation. The cases 1, 2, 4, and 6 correspond to the calculations for the chain length parameter $m = 1, 70, 100,$ and 1000 , respectively, shown in Fig. 11. The cases 3 and 5 correspond to $70 < m < 100$ and $100 < m < 200$, respectively (not shown in Fig. 11). For $m \approx 210$, the gas–liquid critical point crosses the boundary $p^* = 0$ and moves to negative pressure. Legends: solid curves are binodals (the “liquid–liquid” binodals shown in insets 1 and 6 are left out in the other pictures for simplicity of the presentation). Dashed curves are the gas–liquid and “gas–gas” spinodals. The “liquid–liquid” spinodals, which enclose the “liquid–liquid” bin-

odal, are omitted. Symbols denote special thermodynamic states: critical points (CP) (open circles); critical end points (CEP) (filled circles); double critical point (DCP) (filled square); triple points (filled triangles). This series of diagrams explains also how the gas–liquid critical point calculated with PC-SAFT can move to negative pressure for long chains (shown in inset 6).

Fig. 13 Correlation of experimental data for polybutadiene provided by BASF Aktiengesellschaft using PC-SAFT. Circles are polybutadiene data at pressures 0.1, 10, 50, 100, 150, 200 MPa and temperatures 299.14, 317.34, 333.17, 349.08, 365.12, 381.15, 397.2, 413.32, 429.01, 445.27, 461.39 K. Polybutadiene used in these measurements is characterized by $M_w = 45000$ g/mol, 45% cis, 45% trans, 10% 1,2 vinyl. These data were correlated by two sets of molecular parameters. Parameter set 1: $m/M_w = 0.04$, $m = 1800$, $\sigma = 3.467$ Å, $\epsilon/k_B = 280.3$ K (solid curves). Parameter set 2: $m/M_w = 0.0244$, $m = 1098$, $\sigma = 4.065$ Å, $\epsilon/k_B = 257.3$ K (dashed curves). Only the isobars 0.1, 10 and 100 MPa are shown for the parameter set 2. These parameters are provided by BASF Aktiengesellschaft. At low temperature, the calculated density diverges for both sets of molecular parameters. Triangles are the calculations by BASF Aktiengesellschaft for the parameter set 1.

Fig. 14 A comparison of experimental data (symbols) for polybutadiene melt ($M_w = 45000$ g/mol, BASF Aktiengesellschaft) and calculations using the PC-SAFT equation of state (curves). Polybutadiene data were measured at temperatures T_{exp} : 299.14 K, 317.34 K, 333.17 K, 349.08 K, 365.12 K, 381.15 K, 397.2 K, 413.32 K, 429.01 K, 445.27 K, 461.39 K. Calculations using PC-SAFT are shown for the experimental temperatures T_{exp} as well as for the critical “liquid–liquid” isotherm $T_c = 214$ K, a super-critical isotherm at $T = 240$ K and a sub-critical isotherm at $T = 200$ K. PC-SAFT parameters are $m/M_w = 0.04249$, $m = 1912$, $\sigma = 3.389$ Å, $\epsilon/k_B = 269.3$ K. For the high-pressure data, a much too large density is predicted (marked with a dashed circle) as a result of the vicinity of the spurious “liquid–liquid” phase separation predicted by the equation of state. This phase separation (although located at high density and low temperature) affects the correlation and prediction of the experimental data due to increasing

intervals between the isotherms (shown with arrows). The packing fraction values (numbers in brackets) are shown for the x -axis in addition to the density values. These numbers are approximate since the exact values of the packing fraction and the density are related by the diameter, $d(T)$, which is temperature dependent.

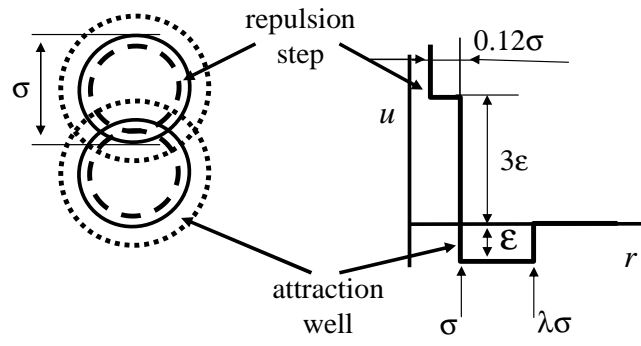


FIG. 1:

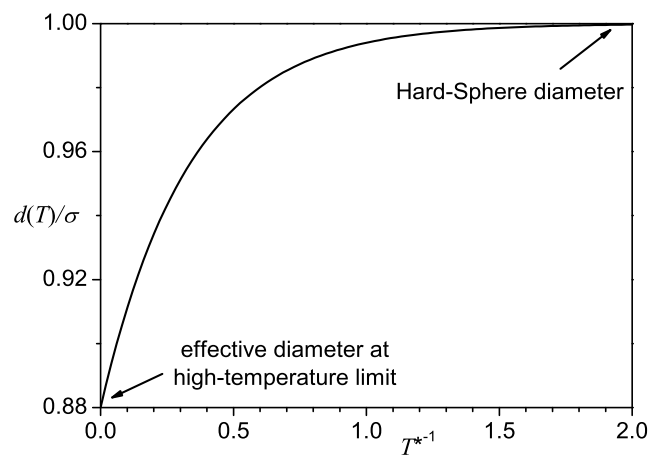


FIG. 2:

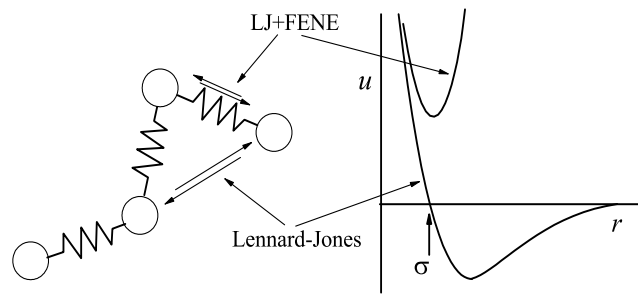


FIG. 3:

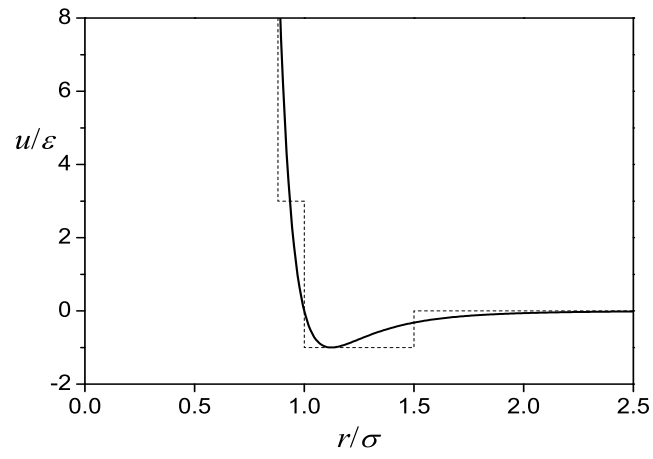


FIG. 4:

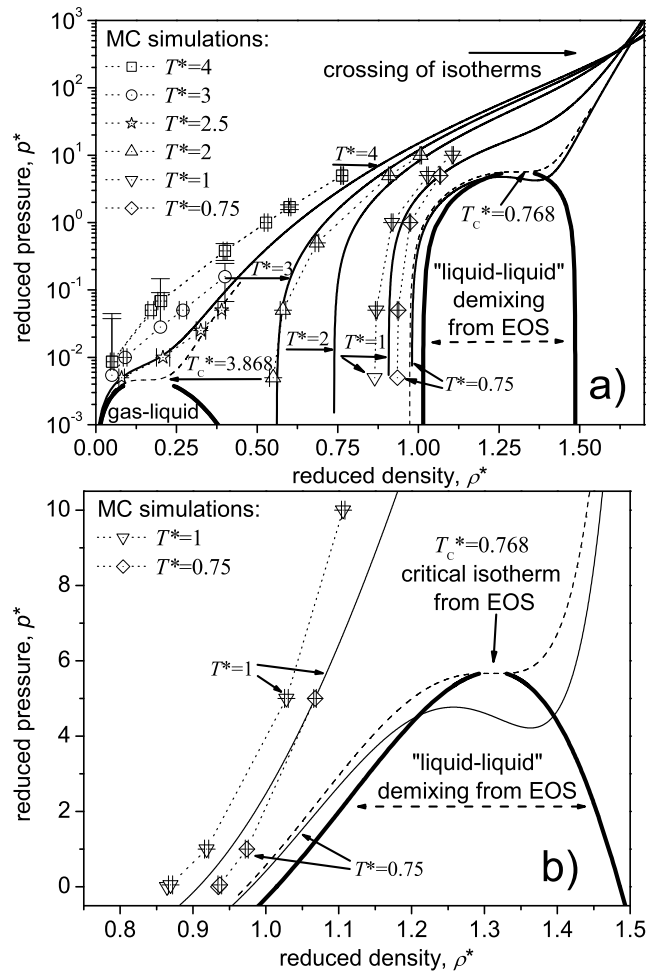


FIG. 5:

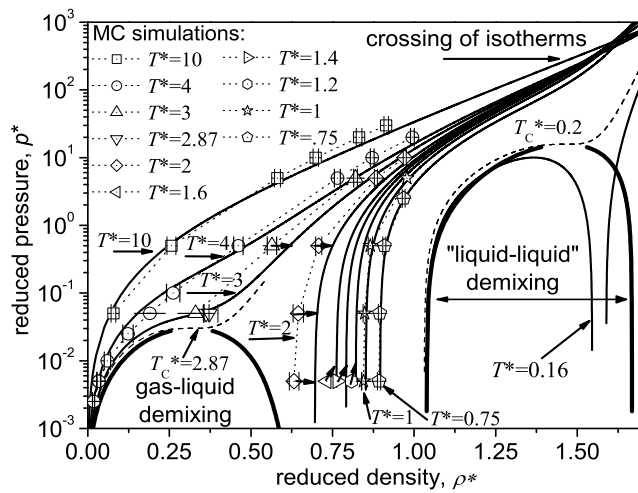


FIG. 6:

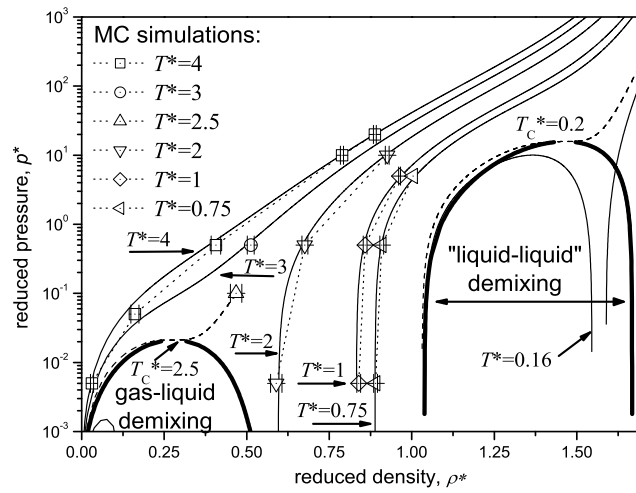


FIG. 7:

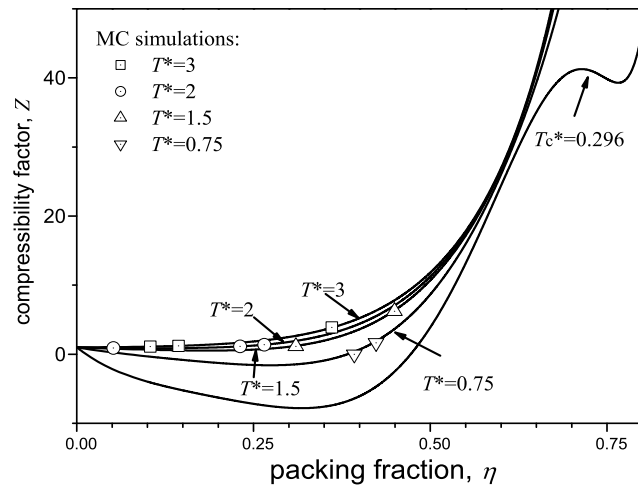


FIG. 8:

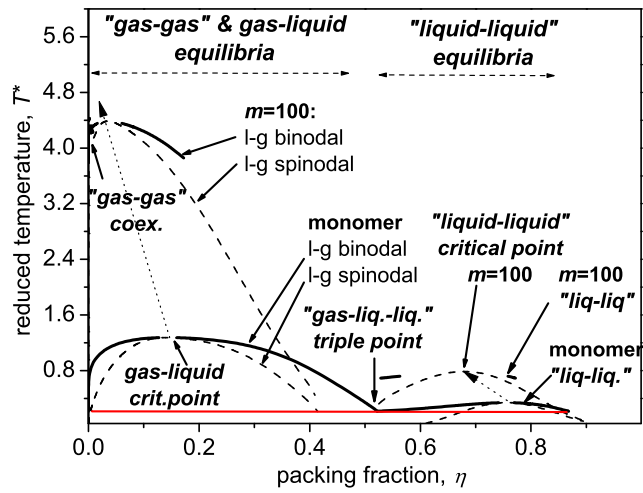


FIG. 9:

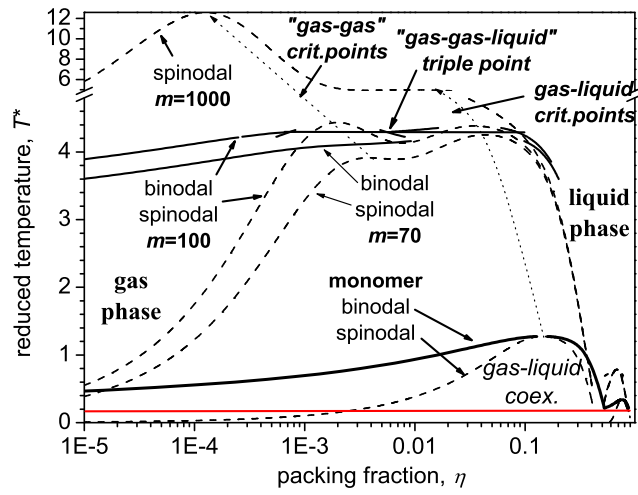


FIG. 10:

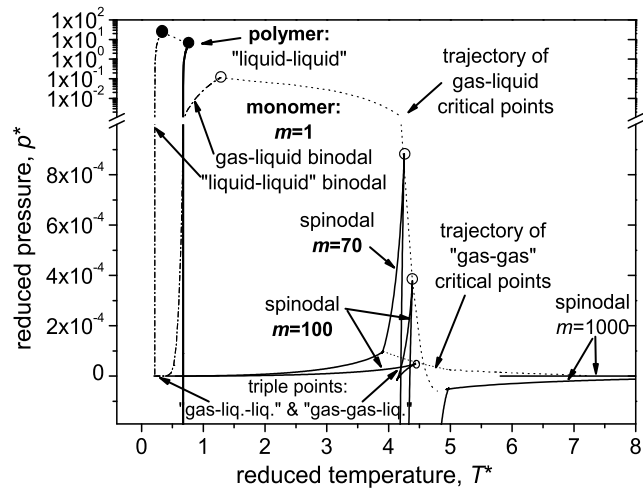


FIG. 11:

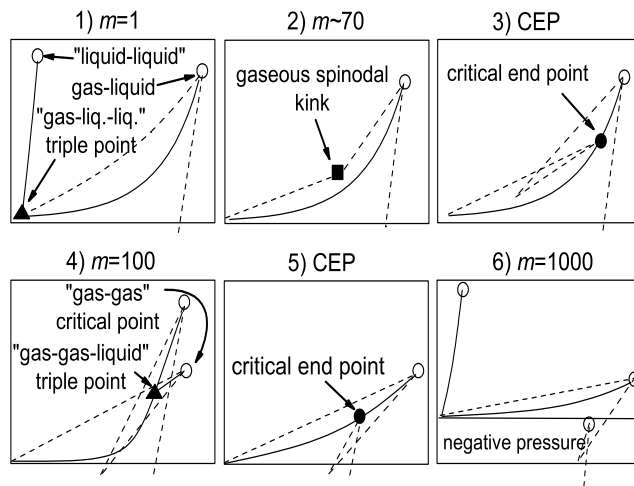


FIG. 12:

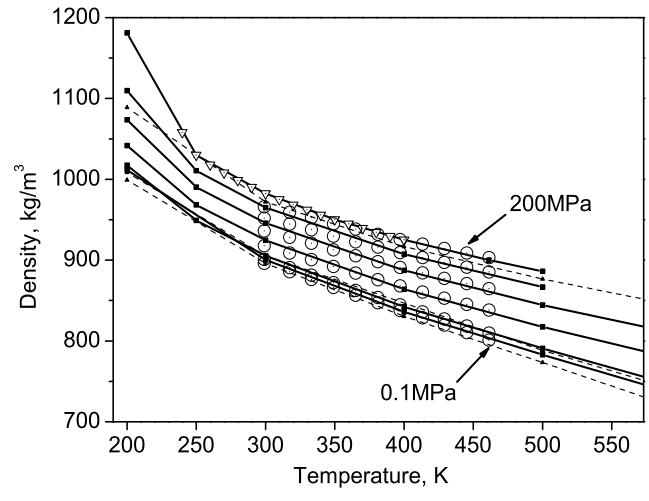


FIG. 13:

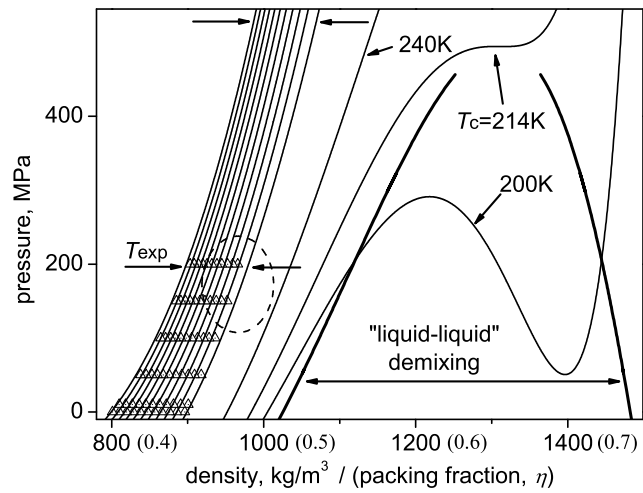


FIG. 14: